Computers and Concrete, *Vol. 16, No. 1 (2015) 125-140*
DOI: http://dx.doi.org/10.12989/cac.2015.16.1.125

Microstructural modelling of the elastic properties of tricalcium silicate pastes at early ages

Huy Q. Do[*1], Shashank Bishnoi[2] and Karen L. Scrivener[1]

[1]*Laboratoire des Matériaux de Construction, Ecole Polytechnique Fédérale de Lausanne (EPFL), Lausanne, Switzerland*
[2]*Department of Civil Engineering, Indian Institute of Technology Delhi, New Delhi, India*

(Received June 20, 2014, Revised July 4, 2015, Accepted July 10, 2015)

Abstract. This paper describes the numerical calculation of elastic properties of a simulated microstructure of cement paste from very early age, when most previous models fail to give accurate results. The development of elastic properties of tricalcium silicate pastes was calculated by discretising a numerical resolution-free 3D vector microstructure to a regular cubic mesh. Due to the connections formed in the microstructure as an artefact of the meshing procedure, the simulated elastic moduli were found to be higher than expected. Furthermore, the percolation of the solids was found to occur even before hydration started. A procedure to remove these artefacts, on the basis of the information available in the vector microstructures was developed. After this correction, a better agreement of the experimental results with calculations was obtained between 20% and 40% hydration. However, percolation threshold was found to be delayed significantly. More realistic estimates of percolation threshold were obtained if either flocculation or a densification of calcium silicate hydrate with hydration was assumed.

Keywords: elastic properties; Ca3SiO5; microstructure; hydration; finite element analysis

1. Introduction

The mechanical properties of cementitious materials, such as their compressive strength and elasticity are important parameters in material and structural design. The strength of the material determines the maximum load that can be safely carried by the structure and the elasticity governs deformations and the serviceability. Understanding and predicting the early-age properties is of practical importance when constructing multi-storied structures as well as being of academic interest. One of the most critical moment in the development of the bearing capacity of cement paste is the setting time. In this study, the setting time is assimilated to the moment elastic stiffness is gained in the microstructure. This also coincides with the moment a continuous solid link is formed between the opposing faces on which the load is applied.

In this article, the elastic properties of C_3S (tricalcium silicate oxide in cement chemistry notation) paste are calculated by applying various techniques on numerically simulated hydrating

[*] Corresponding author, Doctor, E-mail: huy78.do@gmail.com

http://www.techno-press.org/?journal=cac&subpage=8 ISSN: 1598-8198 (Print), 1598-818X (Online)

microstructures. Although similar approaches have been published (Stefan *et al.* 2010, Sanahuja *et al.* 2007, Smilauer and Bittnar 2006) they fail to well reproduce the very early properties, particularly the setting point, when the paste first shows rigid elastic behaviour.

Although easier to measure, compressive strength is, difficult to calculate as it requires complex fracture mechanics. Most available models of compressive strength are empirical and relate it to factors that govern the porosity and its evolution with hydration (Feret 1892, Abrams 1918, Bolomey 1935, Powers 1958). However, the utility of these relationships is limited as they do not take the microstructural features into account. Compressive strength can also be indirectly calculated using empirical relationships with elastic modulus (e.g. ACI Committee 318:2008, EN 1992-1-1:2004), which is relatively easier to simulate numerically.

Several approaches exist for the calculation of homogenised mechanical properties, such as the elastic modulus and Poisson's ratio, of composite materials. Early work in micromechanics used assumptions of uniform strains (Voidt 1887) or uniform stresses (Reuss 1929) to calculate moduli of crystal aggregates. Such assumptions, however, were approximate since in the former approach the forces between grains were not in equilibrium, while in the latter the deformations are not compatible. Still, it was shown that the results from these approaches gave the lower and upper limits for the possible real values of the elastic modulus (Hill 1952). Later work by Eshelby (1957, 1959) modelling the stress field in an elastic medium with an ellipsoidal inclusion, led to the development of various schemes, e.g. the self-consistent scheme (SCS) for the evaluation of multi-inclusion systems (Hill 1965, Mori and Tanaka 1973). These approaches have also been applied to hydrating cement pastes with encouraging results (Sanahuja *et al.* 2007, Bernard *et al.* 2003). These approaches take into account the elastic properties of individual phases and their volume fractions to calculate the overall elastic properties of the composite, making assumptions regarding the arrangement of phases. Although approaches that can take the spatial distribution of inclusions into account have been developed (e.g. Castaneda and Willis 1995), the large number of phases in cements and their complex distribution cannot be analytically modelled.

The arrangement of phases in the microstructure can be explicitly considered through microstructural models that simulate the evolution of cement microstructure with hydration (e.g. Bentz 1995, Bishnoi and Scrivener 2009a). These models can be classified into two main types: discrete and vector. In the former the volume is divided into smaller cubic elements called voxels, each containing one phase that may change with hydration. In the latter approach, the microstructural development is simulated through the growth of layers of products on spherical cement particles and the production of new nuclei in the pores. The discrete approach is computationally less expensive but suffers from a resolution limit that restricts the size of the smallest feature that can be represented in a microstructure. The vector approach is resolution free but is computationally more expensive and is generally limited to spherical particles.

For the calculation of elastic properties, numerical techniques such as the finite element method (FEM) (Hrennikoff 1940, Courant 1943) can be applied directly to the discrete microstructures and to discretised versions of vector microstructures. In FEM, the microstructure is built by joining small elements with uniform properties and the response of the composite material to applied boundary conditions is calculated (Haecker *et al.* 2005). Good estimates of elastic properties can be obtained at later ages using FEM, however, it has been reported that due to the relatively low resolution meshes required due to computational limitations, higher elastic moduli are predicted at early ages as artificial connections between voxels are induced (see Fig. 1) (Haecker *et al.* 2005). It has been shown that the additional connectivity induced due to the limited resolution can be corrected through separation of elements using heuristic rules (Stefan *et al.* 2010, Sanahuja *et al.*

2007). These rules can often be simplistic and it can be difficult to correctly distinguish between the real and artificial connections. Although another method known as the fast Fourier transform (FFT) (Suquet 1990, Moulinec and Suquet 1994) method has also been applied to cements (Smilauer and Bittnar 2006), large contrasts between the elastic properties of phases, e.g. cementitious phases and water, can lead to inaccuracies in the results.

In this article, μic, a vector-based microstructural modelling platform (Bishnoi and Scrivener 2009a), was used to generate three-dimensional hydrating C_3S microstructures that were discretised and analysed using FEM and SCS. All artificial connections due to meshing were removed by explicitly calculating overlaps between the particles in the resolution-free vector microstructure before the final meshing. The elastic properties of the corrected microstructure were calculated using FEM and SCS and were compared with results in the literature (Boumiz *et al.* 2000). It was found that this correction led to an increase in the percolation threshold, defined as the lowest degree of hydration in the simulation where the first chain of connected particles is found. Two different approaches to reduce this threshold were examined in this study. In the first approach, the C_3S particles were assumed to be flocculated in the initial microstructure and in the second approach the packing density of C-S-H was assumed to increase with hydration. This work gives the best estimate yet published of the very early age properties and moreover provides some possible explanations for the setting time as a function of degree of hydration.

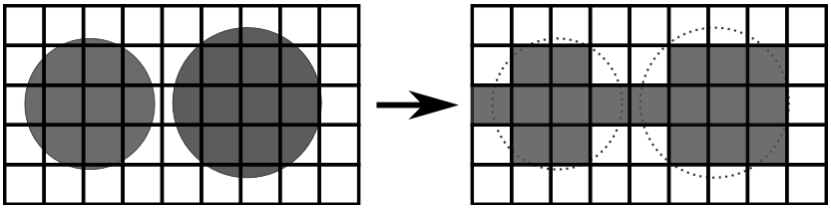

Fig. 1 Artificial connections may be induced due to meshing when distances are smaller than mesh size

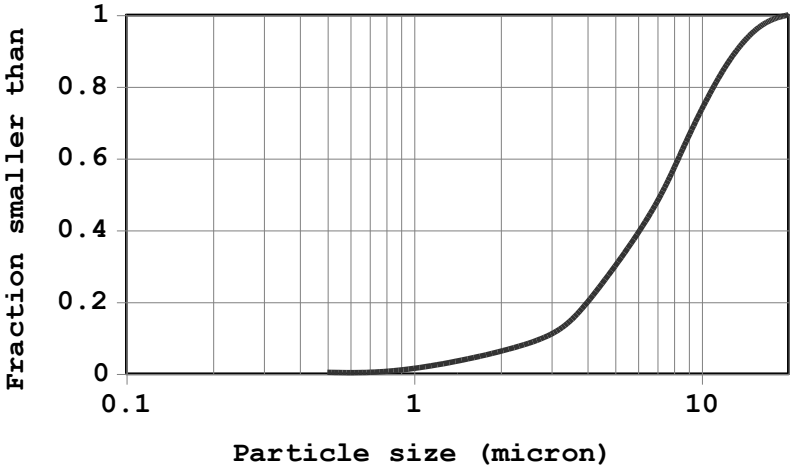

Fig. 2 Particle size distribution of C3S used in the simulations

2. Microstructural model

The open-source modelling platform μic was used to model the hydration of tricalcium silicate ($3CaO.SiO_2$ or C_3S in cement chemistry notation*) pastes – the main phase of portland cements and the resulting three-dimensional microstructure. For interested readers, μic is available at http://micepfl.sourceforge.net/. The advantage of using microstructures from by the μic is that rather generating random spatial distribution of phases, it simulates the processes that lead to microstructural development, generating more realistic representations of microstructures. Additionally, as μic uses the vector approach, the generated microstructures do not suffer from a resolution limit. Although the output of such simulations is often discretised to calculate elastic properties using FEM, the original vector microstructure can be easily used to obtain additional information. In the simulations, spherical particles of C_3S were placed in a computational volume (CV) with 50 μm side having periodic boundaries, using random parking. The effect of flocculation on the development of properties was also studied. The particle size distribution used for C_3S is shown in Fig. 2 and Table 1. This distribution was generated using the median diameter of 8.7 μm and the Blaine's fineness of 400 m^2/kg reported for the powder with which the elastic property results will be compared (Boumiz *et al.* 2000). In order to obtain a representative volume element (RVE) both for hydration and mechanical simulations, the largest unhydrated particle of C_3S was chosen to be 2.5 times smaller than the CV. The diameter of the smallest particle was 0.1 μm (one-fifth of the voxel size of 0.5 μm). Approximately 43,000 particles of C_3S were placed in the 50 μm CV. The hydration of C_3S was simulated by its consumption and the production of calcium silicate hydrate (C-S-H) and calcium hydroxide (CH or portlandite). For each unit volume of C_3S reacting, 1.569 unit volumes of C-S-H and 0.593 unit volumes of CH were assumed to be produced. These numbers are based on specific gravities of 3.15, 2.0 and 2.24 for C_3S, C-S-H and CH respectively and the formula $C_{1.7}SH_4$ for C-S-H. The density of C-S-H of 2.0 g/cm^3 is a typically accepted value including the intrinsic "gel" porosity. As will be discussed below, in some simulations this value was varied. The C-S-H was assumed to grow around the reacting C_3S grains and new particles of CH were created in the pores. The CH particles were produced throughout the first 20 hours of hydration to give a final number of 8,000, which is approximately one-fifth the number of C_3S particles in the system, based on the results published by Jennings and Parrott (1986).

A time-stepping scheme for the simulations was manually entered using trial and error in order to achieve no more than 3% of hydration in each step. Microstructures were produced at various degrees of hydration, starting at 0 and with increments of 0.025 and discretised using a mesh size of 0.5 μm giving a total of one million voxels in the CV. Due to the arrangements of elements at certain degrees of hydration causing locking, some results have been excluded. The mesh size was chosen since little changes in the elastic properties were observed when finer mesh sizes were used. Discretisation was carried out by marking all voxels whose centres are contained inside one of the layers of the cement or hydrate particles as the phase contained in that layer. When multiple particles overlap over the centre of a voxel, the particle that reaches the point earlier in hydration decides the phase of the voxel. When the centre of a voxel does not lie inside any particle, it is considered to be a water-filled pore. It was observed that the discretisation process led to errors in the phase volume fractions of less than 1.5% of the volumes of individual minority phases and less than 0.3% of the total volume of the CV.

---

* Cement chemistry notation: CaO – C; SiO_2 – S; H_2O – H. C_3S is the main phase in Portland cements.

Table 1 Part size distribution of C_3S used in the simulations

Particle size (μm)	Volume fraction smaller than (%)
20	100
15	90
10	75
8	55
5	30
2	12
1	2
0.5	0

Table 2 Intrinsic elastic properties of chemical phases in the homogenization as measured by nanoindentation or mechanical tests (Velez *et al.* 2001, Constantinides and Ulm 2004, Smilauer and Bittnar 2006)

Phase	Young's modulus [GPa]	Poisson's ratio [-]
C_3S	135	0.3
Portlandite	38	0.305
C-S-H average (0.5 low: 0.5 high)	25.55	0.24
Water-filled porosity	0.001	0.499924

3. Homogenisation methods

3.1 Intrinsic elastic properties of chemical phases

The intrinsic elastic properties of the individual phases used in these simulations were taken from the literature (Velez *et al.* 2001, Constantinides and Ulm 2004) and are listed in Table 2. Since a large variation exists in the reported elastic parameters of C-S-H, the average of the values of the elastic modulus reported by Constantinides and Ulm (2004) was assumed for a C-S-H having a density of 2.0 g/cm^3. As discussed later in this article, in order to take the variable density of C-S-H into account, elastic modulus was calculated as a function of the bulk density of C-S-H using SCS. Isotropic linear elastic behaviour and perfect bond between all constituents was assumed.

For computational simplifications, water in saturated condition was modelled to behave as a quasi-incompressible material with an extremely low elastic modulus (see Table 2) and its flow and equalisation of pore pressures were neglected. Because the modulus of water is assumed to be very low, the locking phenomenon, causing an increase in the apparent stiffness of the water elements, does not significantly affect the overall stiffness of the sample. Dunant *et al.* (2013) compared a number of numerical approaches when modelling complex microstructures with high phase property contrast and concluded that the voxel-based approaches produced apparent properties for whole microstructures that were wholly comparable to the ones obtained with conforming meshes.

3.2 Self consistent scheme (SCS)

As discussed earlier, the SCS uses the elastic constitutive law for each phase, the volume

fraction of phases and the average strain or strain concentration tensors of phases to represent the homogenised elasticity tensor. In the most widely used approach by Hill (1965), the strain concentration tensor is estimated by assuming uniform strain induced in an ellipsoidal inclusion in an infinite reference medium subjected to a uniform strain at its boundary, as proposed by Eshelby (1957, 1959). This approach gives good results even at lower volume fractions of the inclusions. In the current study, the inclusions are considered to be spherical and embedded in a medium having the same properties as the homogenised medium. The bulk modulus k_{hom}^{est} and shear modulus μ_{hom}^{est} of the homogenised medium can then be calculated using Eqs. (1)-(4) below.

$$\alpha_0^{est} = \frac{3k_0}{3k_0 + 4\mu_0}; \quad \beta_0^{est} = \frac{6(k_0 + 2\mu_0)}{5(3k_0 + 4\mu_0)} \tag{1}$$

$$k_{\mathrm{hom}}^{est} = \sum_r f_r k_r \left(1 + \alpha_0^{est} \left(\frac{k_r}{k_o} - 1 \right) \right)^{-1} \left\langle \sum_r f_r \left(1 + \alpha_0^{est} \left(\frac{k_r}{k_o} - 1 \right) \right)^{-1} \right\rangle^{-1} \tag{2}$$

$$\mu_{\mathrm{hom}}^{est} = \sum_r f_r \mu_r \left(1 + \beta_0^{est} \left(\frac{\mu_r}{\mu_o} - 1 \right) \right)^{-1} \left\langle \sum_r f_r \left(1 + \beta_0^{est} \left(\frac{\mu_r}{\mu_o} - 1 \right) \right)^{-1} \right\rangle^{-1} \tag{3}$$

$$k_0 \equiv k_{\mathrm{hom}}^{est}; \quad \mu_0 \equiv \mu_{\mathrm{hom}}^{est} \tag{4}$$

In the equations above, k_r, μ_r, k_0 and μ_0 are the bulk moduli and the shear moduli of phase r and of the equivalent medium, respectively. To estimate k_{hom}^{est} and μ_{hom}^{est} in the implicit equation system (1-4) above, an iterative procedure was implemented. Initially, k and μ of the reference medium are estimated as the weighted average of the same parameters of all phases. Alpha and Beta are estimated and applying Eqs. 2 and 3 new k and μ for the reference medium are obtained. The iteration is repeated until k and μ reach a constant value.

Although new approaches have been developed to take the shape of microstructural features into account (Sanahuja *et al.* 2007, Pichler *et al.* 2009), in order to limit the number of fit parameters, the classical SCS approach has been used in this study. This approach is also consistent with that used in the microstructural model, of spherical inclusions in a soft matrix.

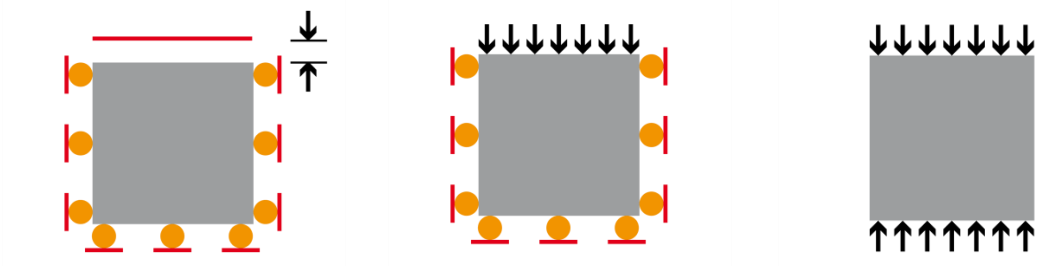

Fig. 3 Boundary conditions: kinematic(left), mixed(centered) and static(right)

3.3 Finite element method (FEM)

FEM is a robust tool for micromechanical analysis that can be conveniently applied even to highly complex microstructures where a discrete mesh can be generated (Hain and Wriggers 2008, Nguyen *et al.* 2012a). In this article, a displacement based FEM is used in which the displacement field is approximated using tri-linear brick elements. An incompatible mesh is chosen because of its low computational complexity and its association with the burning algorithms presented in the next section. The boundary conditions are kinematic, mixed and static uniform boundary conditions shown in Fig. 3. In the kinematic boundary conditions, Dirichlet conditions are applied to perpendicular directions on all faces of the microstructures: five faces prescribed to zero uniform displacements and one face prescribed to non-zero uniform displacements. In the mixed boundary conditions, Dirichlet conditions on five faces to zero uniform displacements still remain, but Neumann conditions are imposed by uniform compressive stresses on the other face. In the static boundary conditions, pure Neumann conditions are applied by imposing uniform compressive stresses with the same magnitude on two opposite faces and the four other faces are free of stress. The Young's modulus and Poisson's ratio are then calculated using the averages of stress and strain fields over the whole CV. Tri-linear shape functions for cubic elements were found appropriate to approximate the displacement field (Smilauer and Bittnar 2006, Haecker *et al.* 2005).

It has been shown that the true elastic properties of a composite material lie between the lower bound calculated using the static boundary condition and the upper bound calculated using the kinematic boundary condition and that the two values converge as the size of the CV tends towards a representative volume element (RVE) (Huet 1990). It will be seen later that since similar results were obtained from both type of bounds, the CV of 50 μm size can be assumed to be representative for the particle size distribution used in this study. For a comprehensive review on the concept of RVE and common boundary conditions used in computational homogenization we refer the reader to (Nguyen *et al.* 2012b).

The simulation of hydration (from 0% to 100%) and FEM with the CV meshed into one million voxels typically took around 10 hours on a desktop computer with CPU 3.0 GHz and 12 GB of RAM. The convergence of finite element conjugate gradient solver is slower at microstructure at lower degrees of hydration and is accelerated after 20% of hydration. This is because the elastic contrasts of phases in the microstructure at low hydration degrees cause high gradients of the displacement field.

4. Simulation of elastic properties

4.1 Comparison with experiments

As discussed earlier, the effective elastic properties were calculated by FEM homogenization using kinematic and static boundary conditions. The results for the kinematic and static boundary conditions are relatively similar (Fig. 4), indicating that in the current case, the CV of 50 μm size can be considered to be representative for the chosen particle sizes (<20 μm) (Pichler *et al.* 2009). Due to faster convergence, the kinematic boundary conditions were applied for calculations in the following sections.

In Fig. 5, the results are compared with experimental results measured by Boumiz *et al.* (2000)

using ultrasonic pulse velocity. A comparison of the results shows that FEM and SCS methods give similar results throughout the range of degrees of hydration studied, even though it has been demonstrated that the results from FEM are affected by the spatial distribution of phases and the results of SCS are not (Castaneda and Willis 1995, Bary *et al.* 2009). Furthermore, it was found that both methods gave a finite elastic modulus even at the first step of the simulation at 2% degree of hydration. This occurs before set was experimentally observed. This is because the artificial connections discussed earlier have not been removed in these simulations, leading to a microstructure that appears to be much stiffer at early ages. It can be seen from the above results that the advantage gained from using microstructure-specific approaches like FEM is lost in comparison to more generalised analytical techniques due to meshing artefacts. The following sections present a technique developed to remove such artefacts before an FEM analysis is carried out.

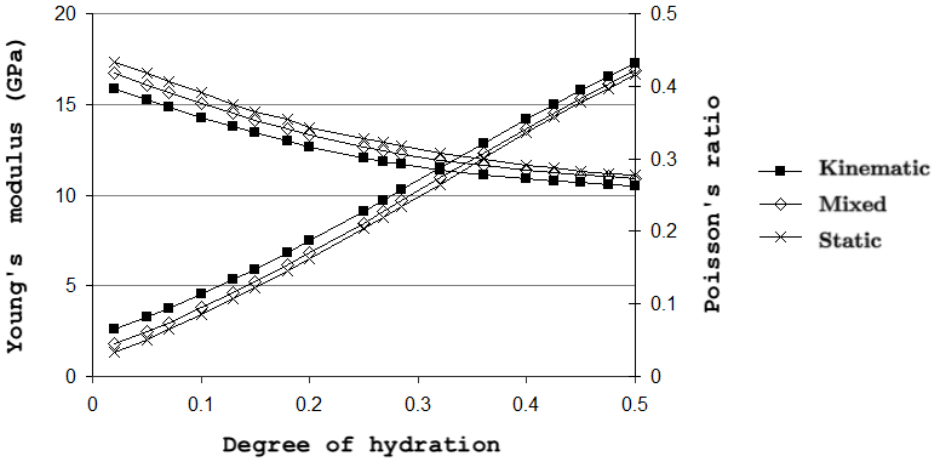

Fig. 4 Comparison of Young's modulus and Poisson's ratio calculated using kinematic, mixed and static boundary conditions

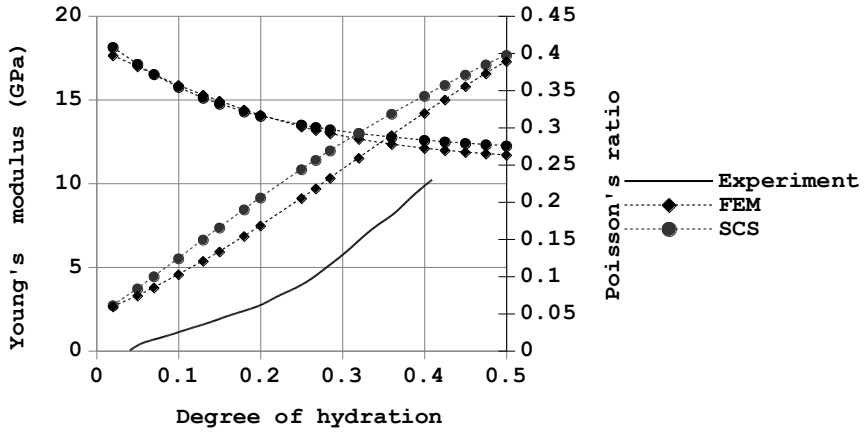

Fig. 5 Elastic properties calculated using different homogenisation techniques

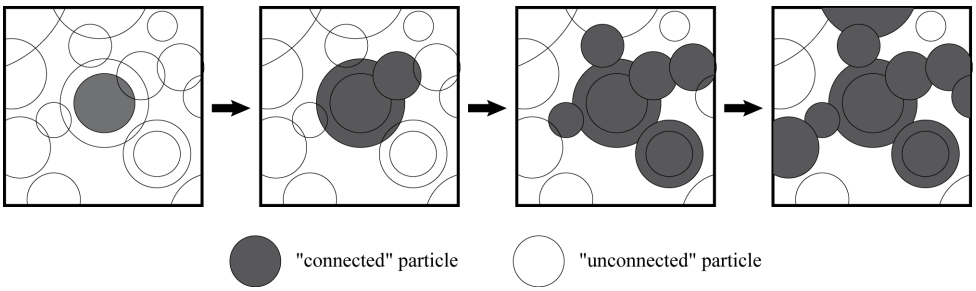

Fig. 6 The process of vector erosion to find connectivity of spheres in the second step of burning applied to a single voxel (represented with the thick black boundary)

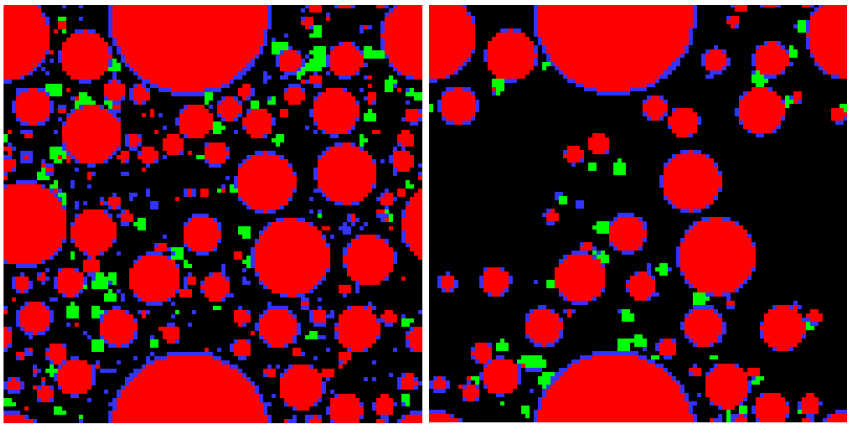

Fig. 7 The meshed microstructure before (left) and after (right) burning. The C3S is in red, the C-S-H in blue and the CH clusters are in green. The porosity and unconnected solids are in black.

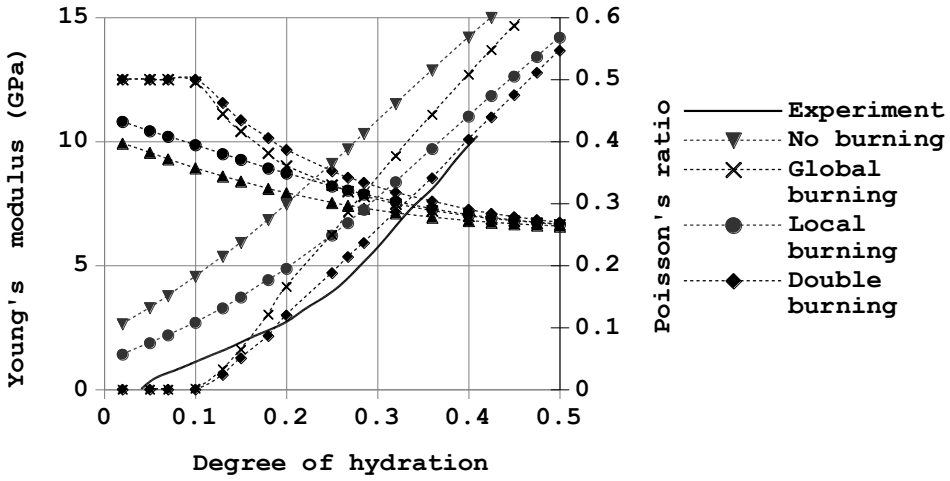

Fig. 8 Effect of global burning, local burning and double burning on elastic modulus calculated using FEM

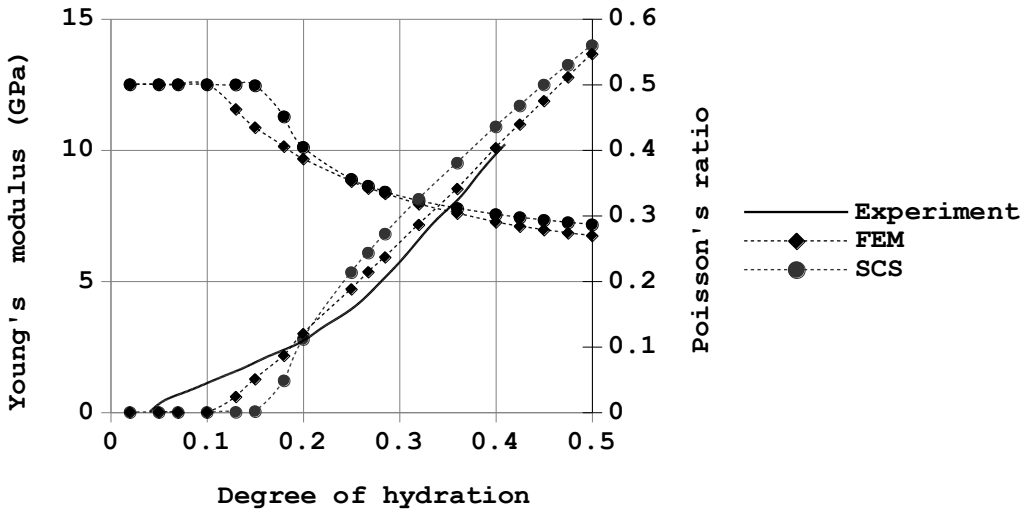

Fig. 9 Elastic properties calculated using different homogenisation techniques after the application of the double-burning algorithm

4.2 Double-burning algorithm

A double burning algorithm was developed to remove the artificial connectivity induced in the microstructures due to the relatively coarse mesh size. This technique uses the vector information available from μic in the form of the centroids and radii of the particles in order to remove artificial connections in two steps. In the first step, known as global burning, all particles that are not connected to at least one of the faces of the CV where the boundary conditions are applied are removed from the microstructure to be discretised. This removes the possibility of disconnected particles appearing to be connecting in the mesh. The first point at which a connected chain of particles is found is known as the percolation threshold. This corresponds to the lowest degree of hydration where elastic properties can be measured. The voxel mesh is then generated using only the particles that have been identified as connected using the procedure discussed earlier. When the centre of a voxel does not lie within a connected particle, it is given the mechanical properties of a water-filled pore.

After the generation of the initial mesh, artificial connections between the remaining particles that appear to be connected in the discretised mesh despite being disconnected in the vector microstructure are removed. In the second step, known as local burning, for each solid voxel, it is verified that a connection exists between two faces of the voxel. This is done by starting from the sphere located at the centroid of the voxel and traversing through all spheres that are connected to this sphere directly or indirectly inside the voxel. If the connected spheres provide a path to move from one face of the voxel to another, always staying within the voxel, the voxel is retained as solid, otherwise it is marked as a water-filled pore. The process of vector erosion to find connectivity of spheres within a voxel is depicted in Fig. 6.

The effect of removing the artificially connected voxels on the microstructure is shown in Fig. 7 and the resulting change in the elastic modulus calculated using FEM is shown in Fig. 8. It is seen in the results that both steps in the double burning process play a role in removing the

artificial connections and lower elastic moduli are observed at lower degrees of hydration. It was observed that for the water to cement ratio studied, the first step of burning had a larger effect on the percolation threshold and the second step has a bigger effect on values after percolation is reached.

It can be seen in Fig. 9 that, although a good agreement with the experiments was observed between 20% and 40% hydration. It was observed (Fig. 9) that the values of elastic modulus calculated from SCS were lower than those calculated from FEM at degrees of hydration below 20%. This is because, although both methods consider similar phase compositions, since all particles that are not present in the percolated chain are removed at lower degrees of hydration, the distribution of the particles is no longer random as assumed in SCS.

In the simulations, percolation was found to occur at degrees of hydration higher than those in the experiments. The above result signifies that in real systems the particles get connected at a lower degree of hydration than in the microstructural model, pointing towards differences between the simulated and real C_3S microstructures, at least at lower degrees of hydration. In order to study the possible cause of these differences, the effect of flocculation of C_3S particles and a variation in the density of C-S-H is studied in the following sections.

4.3 Effect of flocculation of C3S particles

It has been suggested that setting time may be influenced by flocculation (Scherer *et al.* 2012). As the average distance between closest particles in flocculated systems tends to be smaller than systems where particles have been randomly parked, a smaller volume of product and therefore a lower degree of hydration is required to create connections. It was found that the unhydrated cement particles in the simulations formed flocs when the following process was implemented on the microstructure before hydration.

1. Locate the nearest neighbour and find the distance between the surfaces of the two particles.
2. Move the first particle such that the distance between the surfaces of the two particles is halved.
3. Move the first particle in random steps, keeping the distance between the surfaces of the two particles fixed, for a fixed number of steps or until collision with a third particle occurs.
4. Repeat steps 1 to 3 for every particle in the microstructure.
5. Repeat steps 1 to 4 until a stable system is reached.

It was found that the above process has to be repeated 3 times to reach a stable microstructure for the particle size distribution used. Demonstrating the efficacy of the method discussed above, percolation was observed to occur at lower degrees of hydration after the above process was carried out. Simulations carried out at different water-cement ratios using FEM were compared with experimental results from Boumiz *et al.* (2000), as shown in Fig. 10. Although it was found that the degree of hydration at percolation was still slightly higher than the experimentally observed values, flocculation was seen to have a significant effect on the degree of hydration at percolation. It must be noted that SCS cannot be used to study the effect of flocculation as it cannot consider the effect of rearrangement of the particles.

4.4 Effect of C-S-H densification

It has been reported that the packing density of C-S-H is low at lower degrees of hydration and may increase as hydration progresses (Bishnoi and Scrivener 2009b, Thomas *et al.* 2009). Since lower density products occupy larger volumes at similar degrees of hydration, it is expected that

the degree of hydration required for percolation will be lowered as a result of a lower packing density. To study this effect, the variation in the density of C-S-H is modelled in the μic simulation platform by fitting an exponential curve to the average density of C-S-H calculated to match experimentally measured porosity with simulations (0.97 g/cm^3 at 6 hours, 1.38 g/cm^3 at 12 hours, 1.97 g/cm^3 at 3 days of hydration and 2.0 g/cm^3 at 100% hydration) (Do *et al.* 2013). The function obtained using fitting is given in equation 5, where ρ(t) is the density of C-S-H at time t.

$$\rho(t) = 2.0 - \left(\exp(-0.207t) + \exp(-0.054t)\right) \tag{5}$$

SCS homogenisation of C-S-H with lower packing densities was carried out using the properties of the building block of C-S-H described by Jennings (2000) and their elastic properties reported by Constantinides and Ulm (2004) and a relationship between the packing density of C-S-H and its elastic properties was obtained as shown in Fig. 11. A similar process for a smaller range of packing densities of C-S-H has been carried out by Vandamme (2008). Elastic modulus and Poisson's ratio of C-S-H were varied with degree of hydration based on the relationship obtained above to calculate the elastic properties of the paste. As seen in Fig. 12, a good agreement between the experimental results and the calculated elastic modulus could be obtained. Simulations at other water to cement ratios could not be carried out since data on the variation of density of C-S-H with hydration was not available.

The results show that both flocculation and a loosely packed C-S-H can be assumed to obtain a good correlation between experimentally measured and simulated elastic moduli. This indicates that the essential factor in the load-bearing capacity of the cement paste is the connectivity between the phases. As both flocculation and assuming low-density C-S-H produce similar results, it is not possible to decide between these hypotheses in this work.

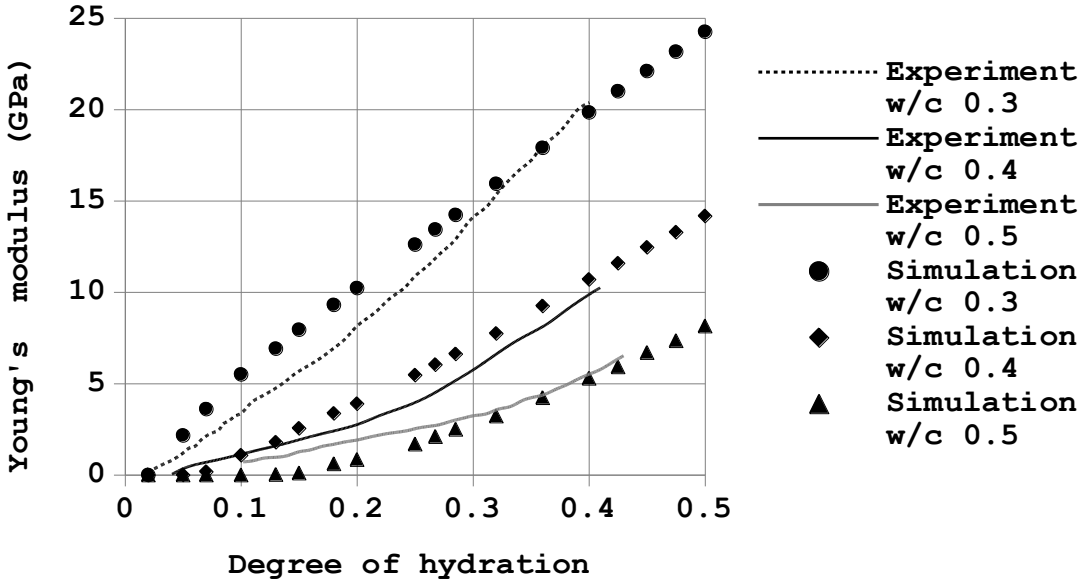

Fig. 10 Effect of flocculation at different water to cement ratios on elastic properties

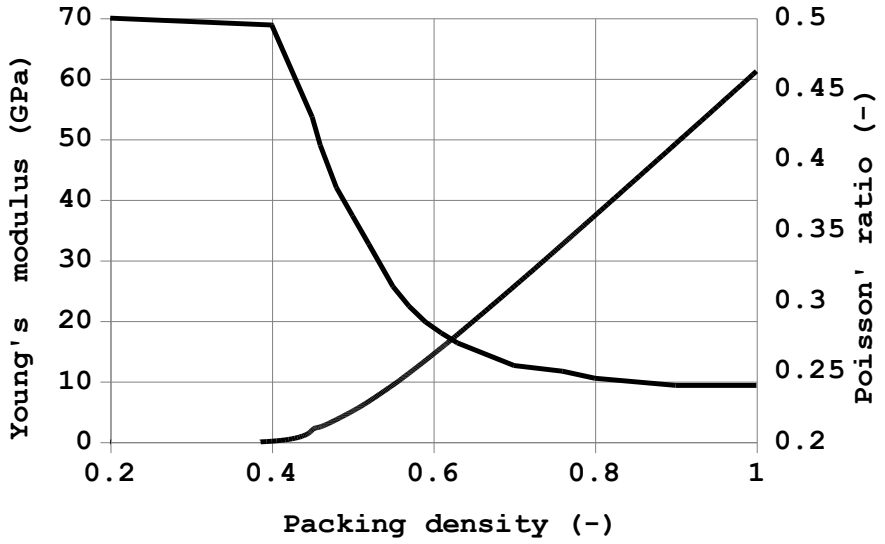

Fig. 11 Effect of packing density of C-S-H on its elastic properties calculated using SCS

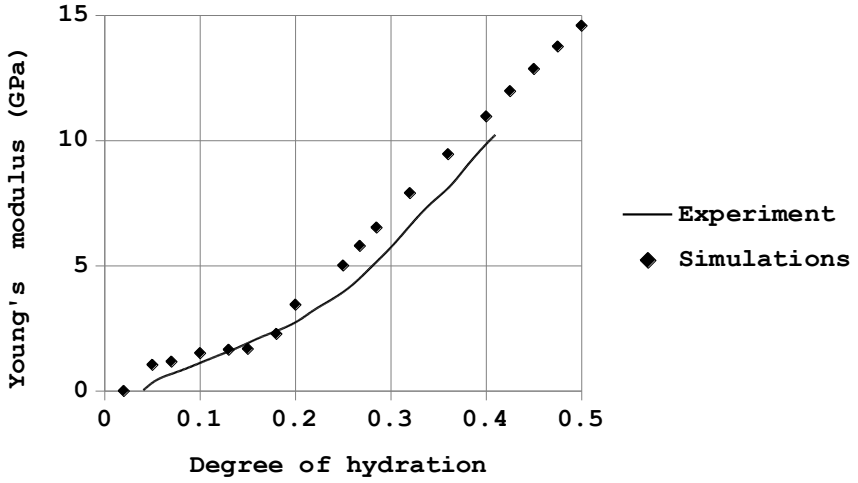

Fig. 12 Comparison of experimental and simulated elastic modulus using finite element simulations for microstructures with variable packing density of C-S-H from SCS shown in Fig. 11

5. Conclusıons

The elastic properties of three-dimensional numerical microstructures of hydrating C_3S pastes were calculated at early ages by applying the finite element method on a discretised numerical microstructure. Higher than expected values of the elastic modulus were found at low degrees of hydration due to artificial connections in the relatively coarse mesh. A method was developed to

remove these artificial connections by using the information available in the resolution-free microstructures available from μic. It was found that after this correction, although percolation takes place at higher than expected degrees of hydration, a good agreement with the experimental results could be obtained between 20% and 40% hydration. A better agreement with the experimental results at lower degrees of hydration could be obtained if the initial microstructure was considered to be flocculated or if a loosely packed C-S-H is assumed to fill a large part of the microstructure and then densify with hydration. It was not possible to distinguish between the two as their mechanical consequences are the same: the formation of bonds which increase the stiffness of the cement paste. The results also show the advantage of using the finite element method over analytical homogenisation techniques as it can more accurately account for the spatial arrangement of the phases. We believe that the approach presented gives the best estimate yet published of elastic properties at very early ages and identifies possible reasons why the setting occurs at the degree of hydration observed experimentally.

Acknowledgments

The authors gratefully acknowledge the financial support from the Swiss National Science Foundation. Authors also thank Dr. A. Guidoum for useful discussions.

References

Abrams, D. (1918), *Design of Concrete Mixtures*, Structural Materials Research Laboratory, Lewis Institute, Chicago, USA.

ACI Committee 318 (2008), *Building code requirements for structural concrete (ACI 318-08) and commentary*, American Concrete Institute.

Bernard, O., Ulm, F.J. and Lemarchand, E. (2003), "A multiscale micromechanics-hydration model for the early-age elastic properties of cement-based materials", *Cement. Concrete. Res.*, **33**(9), 1293-1309.

Bary, B., Ben, M., Adam, E. and Montarnal, P. (2009), "Numerical and analytical effective elastic properties of degraded cement pastes", *Cement. Concrete. Res.*, **39**(10), 902-912.

Bentz, D.P. (1995), *A Three-Dimensional Cement Hydration and Microstructure Program. I. Hydration Rate, Heat of Hydration, and Chemical Shrinkage*, NISTIR 5756, U.S. Department of Commerce.

Bishnoi, S. and Scrivener, K.L. (2009a), "A new platform for modelling the hydration of cements", *Cement. Concrete. Res.*, **39**(4), 266-274.

Bishnoi, S. and Scrivener, K.L. (2009b), "Studying nucleation and growth kinetics of alite hydration using μic", *Cement. Concrete. Res.*, **39**(10), 849-860.

Bolomey, J. (1935), "Granulation et prevision de la resistance probable des betons", *Travaux*, **30**, 228-232.

Boumiz, A., Sorrentino, D., Vernet, C. and Tenoudji, F.C. (2000), "Modelling the development of the elastic moduli as a function of the hydration degree of cement pastes and mortars", *RILEM Proceedings, PRO 13, Hydration and Setting: Why does Cement Set, an Interdisciplinary Approach*, 295-316.

Castaneda, P.P. and Willis, J.R. (1995), "The effect of spatial distribution on the effective behaviour of composite materials and cracked media", *J. Mech. Phys. Solids.*, **43**(12), 1919-1951.

Constantinides, G. and Ulm, F.J. (2004), "The effect of two types of C-S-H on the elasticity of cement-based materials: Results from nanoindentation and micromechanical modeling", *Cement. Concrete. Res.*, **34**(1), 67-80.

Courant, R. (1943), "Variational methods for the solution of problems of equilibrium and vibration", *B. Am. Math. Soc.*, **49**, 1-23.

Do, H.Q., Bishnoi, S. and Scrivener, K.L. (2013), "Numerical simulation of porosity in cements", *Transport. Porous. Med.*, **99**(1), 101-117.
Dunant, C.F., Bary, B., Giorla, A.B., Peniguel, C., Sanahuja, J., Toulemonde, C., Tran, A.B., Willot, F. and Yvonnet J. (2013), "A critical comparison of several numerical methods for computing effective properties of highly heterogeneous materials", *Adv. Eng. Softw.*, **58**, 1-12.
EN 1992-1-1 (2004), *Eurocode 2: Design of concrete structures - Part 1-1: General rules and rules for buildings*, CEN Technical Committee 250.
Eshelby, J.D. (1957), "The determination of the elastic field of an ellipsoidal inclusion, and related problems", *Proceedings of the Royal Society A*, **241**, 376-396.
Eshelby, J.D. (1959), "The elastic field outside an ellipsoidal inclusion", *Proceedings of the Royal Society A*, **252**, 561-569.
Feret, R. (1892), "Sur le compacité des mortiers", *Annales des Ponts et Chaussées*, **7**, 5-164.
Haecker, C.J., Garboczi, E.J., Bullard, J.W., Bohn, R.B., Sun, Z., Shah, S.P. and Voigt, T. (2005), "Modeling the linear elastic properties of Portland cement paste", *Cement. Concrete. Res.*, **35**(10), 1948-1960.
Hain, M. and Wriggers, P. (2008), "Numerical homogenization of hardened cement pastes", *Comput. Mech.*, **42**(2), 197-212.
Hill, R. (1952), "The elastic behaviour of a crystalline aggregate", *Proceedings of the Physical Society*, **65**, 349-354.
Hill, R. (1965), "A self-consistent mechanics of composite materials", *J. Mech. Phys. Solids.*, **13**(4), 213-222.
Hrennikoff, A.P. (1940), "Plane stress and bending of plates by method of articulated framework", Doctoral Dissertation, Massachusetts Institute of Technology, Boston.
Huet, C. (1990), "Application of variational concepts to size effects in elastic heterogeneous bodies", *Mech. Phys. Solids.*, **38**(6), 813-841.
Jennings, H.M. (2000), "A model for the microstructure of calcium silicate hydrate in cement paste", *Cement. Concrete. Res.*, **30**(1), 101-116.
Jennings, H.M. and Parrott, L.J. (1986), "Microstructural analysis of hardened alite paste, part II: microscopy and reaction products", *J. Mater. Sci.*, **21**(11), 4053-4059.
Mori, T. and Tanaka, K. (1973), "Average stress in matrix and average elastic energy of materials with misfitting inclusions", *Acta. Metall. Sin.*, **21**(5), 571-574.
Moulinec, H. and Suquet, P. (1994), "A fast numerical method for computing the linear and nonlinear properties of composites", *Comptes Rendus de l'Académie des Sciences Paris*, II, **318**(11), 1417-1423.
Nguyen, V.P., Stroeven, M. and Sluys, L.J. (2012a), "Multiscale failure modelling of concrete: micromechanical modelling, discontinuous homogenization and parallel computations", *Comput. Method. Appl. M.*, **201-204**, 139-156.
Nguyen, V.P., Stroeven, M. and Sluys, L.J. (2012b), "Multiscale continuous and discontinuous modelling of heterogeneous materials: A review on recent developments", *J. Multi. Model.*, **3**(4),1-42.
Pichler, B., Hellmich, C. and Eberhardsteiner, J. (2009), "Spherical and acicular representation of hydrates in a micromechanical model for cement paste: prediction of early-age elasticity and strength", *Acta. Mech.*, **203**(3-4), 137-162.
Powers, T.C. (1958), "Structure and physical properties of hardened portland cement paste", *J. Am. Ceram. Soc.*, **41**(1), 1-6.
Reuss, A. (1929), "Berechnung der fließgrenze von mischkristallen auf grund der plastizitätsbedingung für einkristalle", *J. Appl. Math. Mech.*, **9**(1), 49-58.
Sanahuja, J., Dormieux, L. and Chanvillard, G. (2007), "Modelling elasticity of a hydrating cement paste", *Cement. Concrete. Res.*, **37**(10), 1427-1439.
Scherer, G.W., Zhang, J., Quintanilla, J.A. and Torquato, S. (2012), "Hydration and percolation at the setting point", *Cement. Concrete. Res.*, **42**(5), 665-672.
Smilauer, V. and Bittnar, Z. (2006), "Microstructure-based micromechanical prediction of elastic properties in hydrating cement paste", *Cement. Concrete. Res.*, **36**(9), 1708-1718.

Stefan, L., Benboudjema, F., Torrenti, J.M. and Bissonnette, B. (2010), "Prediction of elastic properties of cement pastes at early ages", *Comput. Mater. Sci.*, **47**(3), 775-784.
Suquet, P. (1990), "A simplified method for the prediction of homogeneized elastici properties of composites with a periodic structure", *Comptes Rendus de l'Académie des Sciences Paris*, II, **311**, 769-774.
Thomas, J.J., Allen, A.J. and Jennings, H.M. (2009), "Hydration kinetics and microstructure development of normal and CaCl2-Accelerated tricalcium silicate pastes", *J. Phys. Chem. C.*, **113**(46), 19836-19844.
Vandamme, M. (2008), "The nanogranular origin of concrete creep: A nanoindentation investigation of microstructure and fundamental principles of calcium-silicate-hydrates", Doctoral Dissertation, Massachusetts Institute of Technology, Boston.
Velez, K., Maximilien, S., Damidot, D., Fantozzi, G. and Sorrentino, F. (2001), "Determination by nanoindentation of elastic modulus and hardness of pure constituents of Portland cement clinker", *Cement. Concrete. Res.*, **31**(4), 555-561.
Voidt, W. (1887), "Theoretische studien über die elasticitätsverhältnisse der krystalle", *Abhandlungen der Königlichen Gesellschaft der Wissenschaften in Göttingen*, **34**, 3-51.

CC